Ligand signature in the membrane dynamics of single TrkA receptor molecules

Laura Marchetti[1,2,*], Andrea Callegari[1,*], Stefano Luin[1], Giovanni Signore[3], Alessandro Viegi[2], Fabio Beltram[1,3] and Antonino Cattaneo[2,‡]

[1]NEST, Scuola Normale Superiore and Istituto Nanoscienze – CNR, Piazza San Silvestro 12, I-56126 Pisa, Italy
[2]BioSNS Laboratory, Scuola Normale Superiore, c/o Istituto di Neuroscienze del CNR, via Moruzzi 1, I-56100 Pisa, Italy
[3]IIT@NEST, Center for Nanotechnology Innovation, Piazza San Silvestro 12, I-56126 Pisa, Italy

*These authors contributed equally to the work
‡Author for correspondence (antonino.cattaneo@sns.it)

Accepted 3 July 2013
Journal of Cell Science 126, 4445–4456

doi: 10.1242/jcs.129916

Summary

The neurotrophin receptor TrkA (also known as NTRK1) is known to be crucially involved in several physio-pathological processes. However, a clear description of the early steps of ligand-induced TrkA responses at the cell plasma membrane is missing. We have exploited single particle tracking and TIRF microscopy to study TrkA membrane lateral mobility and changes of oligomerization state upon binding of diverse TrkA agonists (NGF, NGF R100E HSANV mutant, proNGF and NT-3). We show that, in the absence of ligands, most of the TrkA receptors are fast moving monomers characterized by an average diffusion coefficient of 0.47 μm^2/second; about 20% of TrkA molecules move at least an order of magnitude slower and around 4% are almost immobile within regions of about 0.6 μm diameter. Ligand binding results in increased slow and/or immobile populations over the fast one, slowing down of non-immobile trajectories and reduction of confinement areas, observations that are consistent with the formation of receptor dimeric and oligomeric states. We demonstrate that the extent of TrkA lateral mobility modification is strictly ligand dependent and that each ligand promotes distinct trajectory patterns of TrkA receptors at the cell membrane (ligand 'fingerprinting' effect). This ligand signature of receptor dynamics results from a differential combination of receptor-binding affinity, intracellular effectors recruited in the signalling platforms and formation of signalling and/or recycling endosome precursors. Thus, our data uncover a close correlation between the initial receptor membrane dynamics triggered upon binding and the specific biological outcomes induced by different ligands for the same receptor.

Key words: TrkA, NGF, proNGF, Lateral diffusion, Single molecule

Introduction

A major open question in cell biology is how different growth-factor receptors achieve molecular specificity even though they activate apparently identical signalling events. Symmetrically, different ligands can activate the same receptor and result in distinct biological outcomes, although bearing similar receptor-binding affinities. Indeed, the mechanisms by which receptors transduce ligand-specific signals are not satisfactorily understood. Here we address this question by studying, at the single molecule level, the dynamics of the neurotrophin receptor tropomyosin-related kinase A (TrkA; also known as neurotrophic tyrosine kinase, receptor, type 1, NTRK1) in the cell membrane of living cells.

TrkA plays a crucial role in the development and survival of sympathetic and sensory neurons, neuronal plasticity, and differentiation of central nervous system cholinergic neurons (Klein et al., 1991; Reichardt, 2006). Although nerve growth factor (NGF) (Levi-Montalcini, 1987) is the main ligand for TrkA, other ligands such as proNGF, the unprocessed form of NGF, and the neurotrophin NT-3 can also activate it. Each of these ligands exerts widely different cellular outcomes, which can only partly be accounted for by a varying contribution from TrkA co-receptor $p75^{NTR}$ (Fahnestock et al., 2001; Harrington et al., 2011; Kuruvilla et al., 2004; Lee et al., 2001). ProNGF can cause actions that are quite opposite to those driven by NGF (Lee et al., 2001) but it might also determine, albeit less effectively than mature NGF, TrkA-dependent neuronal survival (Fahnestock et al., 2001). The recent observation that NGF and proNGF promote different short-term gene expression profiles suggests that they activate different signalling pathways (D'Onofrio et al., 2011); to date, however, the description of the distinct molecular interactions between TrkA and proNGF or mature NGF leading to the observed different biological outcomes is still under debate. NT-3 is known to promote, similarly to NGF, TrkA phosphorylation, and ERK, PLC-γ and Akt signalling activation (Harrington et al., 2011; Kuruvilla et al., 2004), but in contrast to NGF, NT-3 is unable to elicit retrograde-transport-dependent neuronal survival. Moreover, a mutant form of NGF (NGF R100E or 'painless NGF') (Covaceuszach et al., 2010, BBRC; Capsoni et al., 2011) related to the human genetic disease hereditary sensory autonomic neuropathy type V (HSAN V) (Einarsdottir et al., 2004) was shown to bind TrkA with affinity close to that of wild-type NGF, but to activate a specific change in the downstream pathways: that is, a significant, selective reduction of PLC-γ-dependent signalling activation, whereas ERK and Akt pathways are relatively unchanged (Capsoni et al., 2011). This was functionally related to the relative inability of this mutant form of NGF to activate nociceptive pathways.

The dynamics of TrkA in response to NGF was recently studied in living cells by different approaches. GFP-fused TrkA

receptors were imaged in the presence or absence of NGF (Jullien et al., 2003). Membrane movements of *bona fide* NGF–TrkA complexes were investigated at the single-molecule level by NGF conjugated to Cy3 fluorophore (Shibata et al., 2006; Tani et al., 2005) or to quantum dots (Qdots) (Cui et al., 2007; Echarte et al., 2007; Rajan et al., 2008; Sundara Rajan and Vu, 2006). More recently, the simultaneous imaging of a GFP–TrkA fusion and Cy3.5–NGF made it possible to discriminate the retrograde transport of vesicles containing the receptor alone or the ligand–receptor complex (Nomura et al., 2011). However, none of these experimental approaches has yet identified how the lateral mobility of TrkA receptors at the cell membrane and the very early steps of receptor internalization are influenced by the binding of different ligands. Indeed, fusion of GFP to TrkA receptors labels both intracellular and membrane pools, and single receptors cannot be tracked for a sufficiently long time, because of the poor photophysical properties of GFP at the single-molecule level. The alternative use of labelled NGF allows the study of TrkA receptor only in its activated form, so that the net effect of ligand binding on the receptor membrane mobility cannot be investigated. For these reasons, there are still relevant questions that must be explored: are TrkA membrane movements related to ligand-specific receptor activation processes and to the subsequent signalling cascade? How do different ligands affect TrkA dynamics, in comparison to NGF? Are NGF and its precursor proNGF different signalling molecules as far as TrkA binding is concerned?

In the study reported here, by directly imaging single TrkA molecules on the membrane of living cells, we investigated whether and how receptor-membrane dynamics is linked to the specific mode of binding and activation exerted by NGF, 'painless NGF', proNGF and NT-3 ligands. To do so, we exploited a novel strategy to label TrkA (Callegari et al., 2012), which allows imaging and tracking of single receptor molecules both in the absence and in presence of ligands. We provide a quantitative comparison of the diffusive properties and of the oligomeric state of free and NGF-bound TrkA receptors. Moreover, we describe the different receptor-motion patterns induced by the different ligands. TrkA dynamics changes were investigated, also in response to ligands, after inducing a set of biochemical modifications of the cell environment, affecting receptor kinase activity, clathrin-coated pit (CCP) formation, or actin-meshwork integrity. By using a novel single particle tracking (SPT) analysis approach, we demonstrate that the pattern of receptor dynamics in the membrane carries a signature of the ligand by which it was activated.

Results

Individual ACP–TrkA trajectories display different dynamic regimes at the membrane of SH-SY5Y cells

We recently demonstrated that the acyl carrier protein (ACP) fused at the N-terminus of TrkA preserves the full functional responsiveness and signalling activation of the receptor, and allows its imaging at the single-particle level in the plasma membrane of living cells (Callegari et al., 2012). Here, the ACP–TrkA construct was transiently transfected into undifferentiated SH-SY5Y neuroblastoma cells. The receptor pool at the cell surface was selectively labelled by biotinylation of the ACP tag and subsequent addition of streptavidin-coated Qdots (S-Qdots) emitting at 655 nm. Bulk labelling was obtained using a concentration of 20 nM S-Qdots in the final labelling step. Fig. 1A shows our typical microimages: cells expressing the construct display S-Qdot red staining on the plasma membrane, whereas the cell body is green as a result of the simultaneous expression of GFP (the latter was inserted in the same expression plasmid). In order to detect and track single ACP–TrkA molecules in the cell membrane, we lowered the S-Qdots concentration down to 2 nM and selectively imaged the basal membrane of the cells facing the coverslip by total internal reflection fluorescence (TIRF) microscopy (Fig. 1B). We analysed cells displaying 5–50 dots on the basal membrane (0.01–0.1 dots/μm^2), as occurred with the same labelling reaction in the case of a SH-SY5Y stable cell line expressing low levels of the ACP–TrkA construct. The density of labelled receptors is an important issue when performing SPT studies (Jaqaman et al., 2011; Kasai et al., 2011) and in our case the selection of cells with low-expression profile of the construct is necessary also to avoid autoactivation of the receptor kinase activity in the absence of NGF (supplementary material Fig. S1). The use of S-Qdots as a probe allowed long-term tracking of individual ACP–TrkA receptors and revealed a rather heterogeneous behaviour. A pool of receptors was almost immobile during the whole observation period (Fig. 1C); long trajectories also showed multimodal dynamics, switching from periods of faster diffusion to phases of transient arrest of lateral diffusivity (Fig. 1D). TAD (transient arrest of diffusion) analysis was performed to separate trajectory segments corresponding to confinement regions from those corresponding to diffusive or drifting traits. The resulting subtrajectories, if not assigned to TAD events, were pooled together with other receptor trajectories (usually shorter than the multimodal ones) that displayed a unique mode of diffusion: either slow or fast diffusing, sometimes within a confinement area and, more rarely, drifting (Fig. 1E, top, middle, bottom panels respectively). The quantitative parameters describing all classes of trajectories and subtrajectories and their respective frequency are summarized in Table 1 and further explained in the Materials and Methods and in supplementary material Fig. S7; supplementary material Table S1 summarizes the results arising from multimodal trajectories only. The whole set of monomodal trajectories and subtrajectories analysed are hereafter referred to as (sub)trajectories, and their numbers are reported in the column '(sub)traj' of Table 1.

NGF binding decreases TrkA diffusivity and confinement length

The lateral mobility of ACP–TrkA was first investigated in the absence and presence of saturating concentrations of NGF (125 ng/ml). The ligand was added to the cell medium and receptor mobility was monitored immediately afterwards, within a time window of 15 minutes. We found that NGF binding to TrkA resulted in macroscopic clustering of receptor molecules (Fig. 2A) and in a decrease in its diffusivity (Fig. 2B,C; Table 1). When analysing the immobile receptor population (Fig. 1C), we observed that NGF addition causes an eightfold increase in the total time–length fraction of these trajectories from 3.8% to 29.7% (Table 1); furthermore, the average confinement length $<L>$ of immobile receptors is halved upon ligand binding, from 0.59 ± 0.08 μm to 0.29 ± 0.02 μm (uncertainty: s. e.; Fig. 2B). As for the TAD events and the slow and fast diffusing TrkA trajectories (Fig. 1D–E), no significant variation of their confinement length was observed, whereas their total time–length frequency was redistributed: both TAD events and

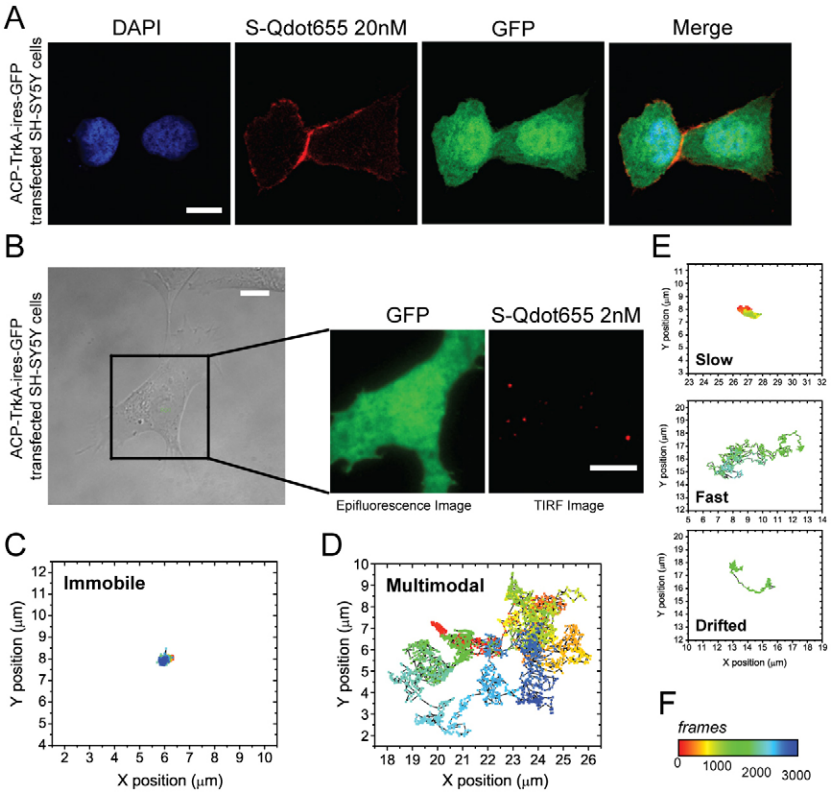

Fig. 1. Selective labelling of membrane-localized ACP–TrkA receptor for SPT experiments. (A) Confocal images of SH-SY5Y cells transiently transfected with ACP–TrkA-IRES-GFP construct. The green channel is GFP fluorescence; the red channel is ACP–TrkA receptor at the cell membrane after its biotinylation and subsequent conjugation with 20 nM S-Qdots655. Scale bar: 10 μm. (B) Typical S-Qdots distribution on the basal membrane of living SH-SY5Y cells maintained at 37℃ upon labelling of biotinylated ACP–TrkA with 2 nM S-Qdots (red channel, imaged by TIRF; DIC transmission microscopy image in grey and epifluorescence GFP channel in green are shown as references). Scale bar: 20 μm in grey channel; 10 μm in red and green channels. (C–E) Representative trajectories of tracked receptors, with spot colour coding for the frame number (3000 frames being 63 seconds). Trajectories were classified into different diffusive categories, e.g. immobile (C) or multimodal (D); the latter ones may be composed of subdiffusive or slow (E, top panel), free diffusive or fast (E, middle panel) and superdiffusive or drifted (E, bottom panel) dynamics modes. (F) Colour-coded map representing the frame number for spots in the trajectories.

slow-diffusing trajectories increase by a factor 1.7, while fast-diffusing receptor molecules were halved upon NGF addition (Table 1). Similarly, both the total time fraction and length of the drifted trajectories were shortened by NGF treatment (Table 1). We recorded a bimodal behaviour in the distribution of the diffusion coefficient D of non-immobile TrkA receptors (Fig. 2C), both in the absence and in the presence of NGF. Notably, NGF addition causes a 1.7-fold decrease of the integral of the peak corresponding to faster diffusion and a 2.4-fold increase of the integral of the lower-diffusivity peak, together with a marked increase in the separation of the two peaks.

NGF binding induces receptor di- or oligomerization

In order to assess whether and how the receptor oligomeric status is related to the above-described changes of lateral diffusion, we changed the labelling of the receptor and covalently conjugated a CoA derivative of the Atto633 fluorophore (CoA-Atto633) to the ACP–TrkA expressed at the membrane of SH-SY5Y cells. Indeed, organic fluorophores produce more monodispersed photophysical features than Qdots, and thus are more suitable to directly link the fluorescence intensity of the tracked objects to the oligomeric forms of the receptor (Resch-Genger et al., 2008). The average intensity for single fluorophores measured with our TIRF microscope set-up was around 3000 arbitrary units in all our experiments. As an example, the left panel in Fig. 2D shows the intensity signal recorded in the case of a spot comprising two fluorophore molecules whose individual bleaching can be monitored.

In order to analyse correlations between oligomeric status and the diffusion coefficient of Atto633-labelled TrkA receptors, we plotted the two-dimensional (2D) distribution of D and spot intensity $<I>$ averaged on each trajectory (Fig. 2D). In the case of unstimulated receptors, the peak of this 2D distribution lay at an $<I>$ value corresponding to single molecules and at a D value consistent with the fastest mobile population of TrkA (Fig. 2D, central panel). From these data we conclude that about 70% of TrkA receptors (as calculated from the integral of the distribution in the central panel of Fig. 2D within the black rectangle) is present as fast diffusing monomers at the cell membrane in the absence of any ligand. The remaining detected particles, with lower mobility, appeared to have variable intensities spanning values between the ones expected for monomers and dimers or, albeit very infrequently, larger oligomers. When imaging in the presence of NGF was performed, the intensity of tracked Atto633-ACP–TrkA molecules displaying both fast and slow diffusion was significantly modified (Fig. 2D, right plot). On the one hand, the fast population of tracked receptors had a more heterogeneous average intensity, with values intermediate between the intensity of monomeric and dimeric receptor forms (indicated by the two white crosses on the graph). This is probably a result of the monomer–dimer equilibrium undergone by the TrkA receptors upon ligand stimulation (or possibly by the photobleaching of a single fluorophore in a dimer). Indeed, the shift towards the dimer fluorescence intensity corresponds to a slight decrease of D, possibly linked to the increase of the molecular mass of the tracked objects and/or to interactions with sub-membrane effectors. On the other hand, the receptor population with lower diffusivity was not only greatly increased (in agreement with data reported in Fig. 2B,C), but also showed a wide range of average fluorescence intensities, spanning from monomers to oligomers containing up to about eight individual receptor molecules.

Table 1. Quantitative parameters describing ACP–TrkA single molecule dynamics in response to different stimuli

					Immobile					TAD events					
Treatment	*n*	No.trajs	Multi	(Sub)trajs	Trajs	Time%	$<t>$ (s)	$<L>$	ΔL	Trajs	Time%	$<t>$ (s)	τ (s)	$<L>$	ΔL
TrkA, untreated	32	350	112	677	13	3.8	13.1	0.59	0.29	190	10.1	2.4	0.4	0.56	0.50
TrkA+NGF	31	531	123	909	121	30.2	26.8	0.29	0.23	243	17.9	7.9	0.4	0.47	0.55
TrkA+NGF R100E	22	647	159	1263	121	27.0	30.0	0.34	0.23	392	19.3	6.6	0.4	0.61	0.56
TrkA+proNGF	19	630	173	1234	59	16.3	26.2	0.40	0.28	375	20.0	5.0	0.4	0.45	0.42
TrkA+NT-3	16	529	221	1520	37	11.4	24.9	0.39	0.20	564	16.4	2.3	0.6	0.37	0.36
TrkA+K252a	14	437	121	854	60	18.2	20.2	0.41	0.25	262	19.6	5.0	0.5	0.44	0.44
TrkA+K252a+NGF	27	1002	306	2077	99	14.9	25.0	0.32	0.23	633	14.4	3.8	0.5	0.44	0.43
TrkA+Chlprz	19	491	202	1152	17	5.3	17.6	0.32	0.24	371	14.6	2.2	0.5	0.28	0.34
TrkA+Chlprz+NGF	22	728	269	1546	69	15.5	19.4	0.34	0.25	491	16.6	2.9	0.6	0.36	0.45
TrkA+CytD	17	612	223	1274	94	25.2	25.4	0.38	0.23	421	19.8	4.5	0.9	0.35	0.48
TrkA+CytD+NGF	13	326	87	686	92	35.6	27.5	0.36	0.24	219	16.2	5.3	0.6	0.42	0.43

	Slow					Fast					Drifting			
Treatment	Trajs	Time%	$<t>$ (s)	$<L>$	ΔL	Trajs	Time%	$<t>$ (s)	$<L>$	ΔL	Trajs	Time%	$<t>$ (s)	τ (s)
TrkA, untreated	20	11.0	24.5	0.9	1.1	437	72.7	7.5	3.3	2.2	17	1.9	6.0	7.7
TrkA+NGF	87	19.4	24.0	0.8	0.5	433	31.6	8.3	3.4	2.3	25	0.7	3.9	3.4
TrkA+NGF R100E	115	18.7	21.9	1.1	0.9	605	34.2	8.3	2.8	1.7	30	0.4	4.0	1.6
TrkA+proNGF	48	8.5	16.7	0.8	0.4	722	53.8	7.4	3.7	3.0	30	0.8	4.3	5.7
TrkA+NT-3	30	7.0	18.9	0.8	0.6	869	64.3	6.7	2.6	1.6	20	0.2	1.1	2.1
TrkA+K252a	56	13.5	16.1	1.0	0.5	444	46.1	7.2	2.9	1.7	32	2.0	4.1	1.7
TrkA+K252a+NGF	58	8.2	23.4	1.6	1.9	1258	61.1	8.4	3.5	2.8	29	0.8	10.3	2.8
TrkA+Chlprz	16	3.2	11.2	2.4	2.1	729	76.1	6.0	2.9	1.6	19	0.3	1.0	1.0
TrkA+Chlprz+NGF	54	7.5	12.0	1.0	0.7	909	59.7	5.8	2.8	2.0	23	0.3	2.1	1.7
TrkA+CytD	62	12.5	19.1	1.0	0.4	660	41.1	6.1	2.7	1.8	37	0.5	2.4	4.5
TrkA+CytD+NGF	49	22.5	32.7	0.5	0.4	303	23.6	5.7	2.4	1.3	23	1.3	8.1	2.7

n, number of cells analysed; No.trajs, number of trajectories detected; Multi, number of multimodal trajectories detected; (Sub)trajs, total number of trajectories and subtrajectories after TAD analysis; Trajs, total number of (sub)trajectories of each type; Time%, total time fraction for the (sub)trajectory type; $<t>$, average trajectory time length; τ, parameter in the exponential fit for the distribution of the time lengths of the trajectories (reported for TAD events in order to reduce the impact of long slow or immobile subtrajectories that were actually the most part of a trajectory; in the other cases it is not significantly different from $<t>$); $<L>$ and ΔL, average and s.d. of the distributions for the confinement length L considering only the (sub)trajectories where L is in agreement with the calculated s.d., σ_r for the *x*-*y* positions in the corresponding trajectory ($1.25<L/\sigma_r<4.75$).

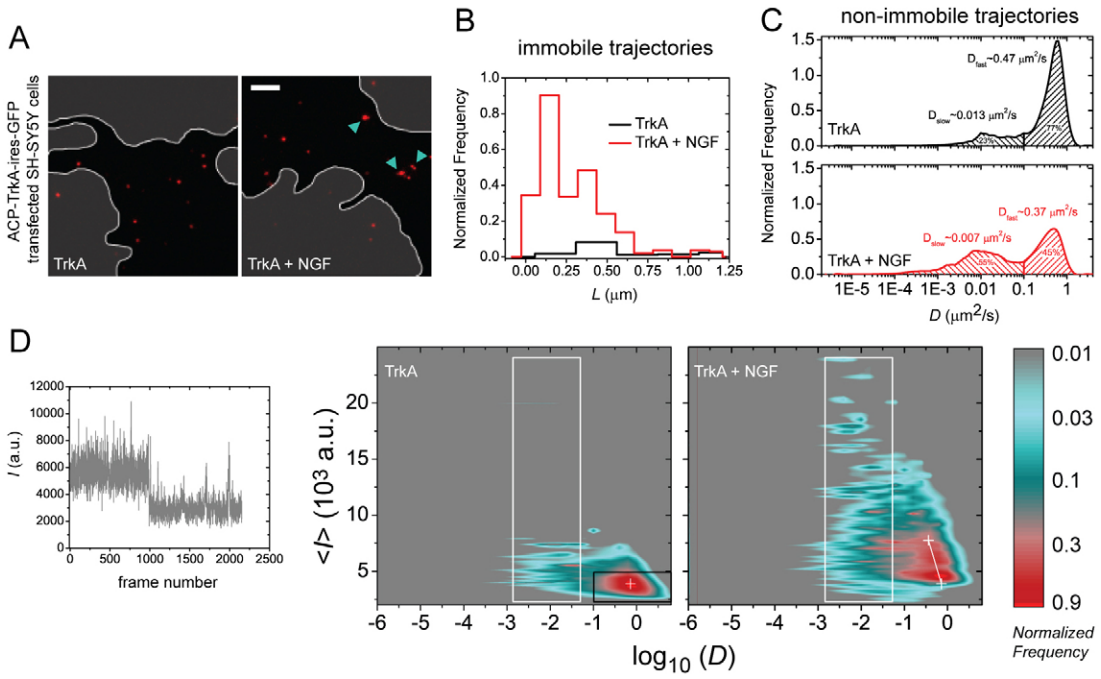

Fig. 2. Effects of NGF on ACP–TrkA mobility at 37°C. (A) TIRF microimages showing the distribution of ACP–TrkA receptor labelled with 2 nM S-Qdots655 before (red channel, left panel) and after NGF administration (red channel, right panel) at the SH-SY5Y plasma membrane. Areas outside cells are shown in grey. NGF-induced receptor clustering is indicated by arrowheads in right panel; scale bar: 5 μm. (B) Distributions of the receptor confinement length *L* for 'immobile' trajectories of S-Qdot-labelled ACP–TrkA receptors in the presence (red curve, $n=121$) or absence (black curve, $n=13$) of NGF, with areas under the curve normalized to the fractions of spots assigned to immobile trajectories. (C) Distribution of the short-lag-time diffusion coefficient (*D*) of S-Qdot-labelled ACP–TrkA receptors for non-immobile trajectories in the presence (red curve, $n=788$) or absence (black curve, $n=664$) of NGF. The areas under the reported distributions are normalized to the fraction of spots in non-immobile trajectories. The percentages were calculated considering the areas under the curve above and below $D=0.1$ μm^2/second. (D) Fluorescence intensity (*I*) analysis of single Atto633 molecules and Atto633-labelled ACP–TrkA observed by TIRF microscopy. Left panel: typical time-course of *I* for a spot comprising two molecules of the organic dye CoA-Atto633 adhered to the bottom of the Petri dish. Right panels: 2D distribution of the average fluorescence intensity $<I>$ of Atto633-labelled ACP–TrkA trajectories and of *D* in the untreated (central panel, $n=7367$) and NGF-treated (right panel, $n=10{,}288$) cases. NGF treatment induces receptor dimerization within higher-*D* trajectories (the white line connects the fluorescence intensity of the monomer to that of the dimer, which appears to have a halved *D*) and oligomerization (white rectangular area) corresponding to increased average fluorescence and decreased diffusivity of receptor aggregates.

Effect of other TrkA ligands on TrkA lateral diffusion

We next investigated how TrkA receptor dynamics is influenced by three other ligands (whose biological effect through TrkA binding is summarized in supplementary material Fig. S2): a mutant form of NGF bearing the R100E point mutation (NGF R100E), the unprocessed pro-neurotrophin proNGF, and the neurotrophin NT-3. The distributions of confinement length and of *D* values obtained from the analysis of tracked receptors in the three cases are reported in Fig. 3, A–C and D–F, respectively (data obtained for TrkA in the absence and in the presence of NGF are also reported in each panel as a reference). We found that all ligands induce increased immobilization (Fig. 3A–C; Table 1) and a redistribution between the two peaks of TrkA diffusion in favour of the lower diffusivity one (Fig. 3D–F; Table 1) when compared to the non-stimulated receptor. However, whereas NGF R100E induced an increase of the total time fraction of both TAD events and slow trajectories in a similar way to NGF, proNGF and NT-3 elicited the increase only of TAD occurrence (Table 1, columns Time% of TAD events and slow trajectories). Clearly, the extent of receptor mobility modification is very different for the various ligands, with NGF R100E having the highest similarity to the NGF-driven behaviour, and proNGF and NT-3 being substantially different from NGF.

In order to better evaluate the differential effects exerted by the four analysed ligands when compared with each other and with the non-stimulated receptor, we generated the 2D distribution of two parameters summarizing the diffusive behaviour of all (sub)trajectories obtained for each case (Fig. 4). These parameters are the *D* coefficient, and the γ coefficient calculated using the MSS algorithm (Ewers et al., 2005): the smaller the γ value, the more sub-diffusive is the motion of the receptor (as it is for confined ones), with a theoretical $\gamma\sim0.5$ for free-diffusing particles and $\gamma>0.5$ for drifted ones. All graphs were divided into eight dynamics regions (delimited by the grey rectangles numbered in Fig. 4A) and the relative weight of trajectories within each region was quantified and reported as a stack-column graph in Fig. 4G (and as percentages in supplementary material Table S2). It is evident that NGF and NGF R100E induce the most prominent shift towards the slow-diffusing receptor pool (regions 2–3) and the almost-immobile receptors fraction (regions 4–6); however, this analysis reveals a subtle difference, in that the slower trajectories are differently redistributed in the D-γ distributions for these two ligands. ProNGF has a slowing effect on TrkA mobility similar to that of NGF, but weaker; finally NT-3-induced D-γ distribution resembles that of the receptor in the absence of any ligand,

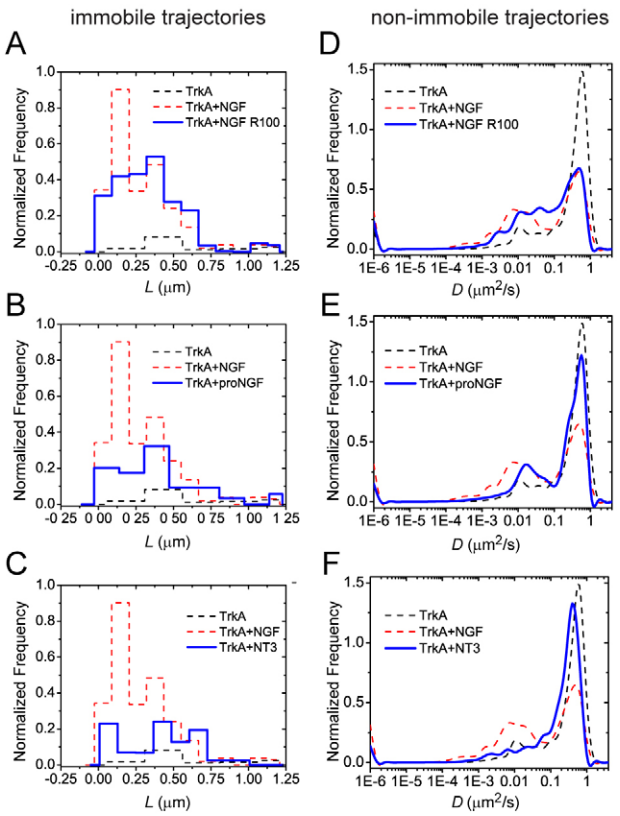

Fig. 3. Effect of ligands on ACP–TrkA mobility. (A–C) Distributions of the confinement length *L* for 'immobile' trajectories of S-Qdot-labelled ACP–TrkA receptors (blue curves) upon treatment with NGF R100E mutant (NGF R100; A; $n=121$), pro-NGF (B; $n=59$) and neurotrophin-3 (NT-3; C; $n=37$). Normalization as in Fig. 2B, whose content is reproduced here as dashed curves for comparison. (D–F) Diffusion coefficient (*D*) distribution (blue curves) of non-immobile trajectories of S-Qdot-labelled ACP–TrkA receptors upon treatment of cells with NGF R100E (D; $n=1142$), pro-NGF (E; $n=1175$) and NT-3 (F; $n=1483$). Normalization as in Fig. 2C, whose content is reproduced here as dashed curves for comparison.

except for a higher population in region 5 and a lower one in region 2. This analysis highlights the existence of distinct, ligand-dependent modes of diffusion and confinement for ACP–TrkA upon ligand stimulation.

TrkA lateral mobility is modified by drug treatments affecting TrkA kinase activity, the early events of endocytosis and the actin meshwork

We next investigated how the different motion and diffusivity patterns described in the previous section depend on the TrkA receptor state and/or on the structural components of the plasma membrane. We first took into account the intrinsic receptor kinase activity. SH-SY5Y cells transfected with ACP–TrkA construct were treated overnight with the kinase inhibitor K252a, which resulted in the complete inhibition of ACP–TrkA phosphorylation (supplementary material Fig. S3A). Cells were then labelled with S-Qdots and individual receptor molecules imaged either in the absence or in the presence of NGF. K252a treatment affected the mobility of the receptor, mainly by increasing the population in diffusivity region 3 (Fig. 5A,G); more importantly, this treatment dramatically impaired the observed NGF-induced receptor slowing down and immobilization (Fig. 5B,G; Table 1; supplementary material Fig. S4A,B; Table S2).

We then investigated how inhibition of CCPs formation affects TrkA membrane mobility and NGF-associated alterations in TrkA diffusion patterns. To this end, SH-SY5Y cells transfected with ACP–TrkA construct were treated with chlorpromazine (Chlprz), a selective inhibitor of CCP formation and of clathrin-dependent early endocytosis, as assessed by the impairment of Alexa-Fluor-488-labelled transferrin internalization in SH-SY5Y cells (supplementary material Fig. S3B). We found that this treatment also had only a slight effect onto TrkA lateral mobility in resting conditions (Fig. 5C,G), mainly decreasing the slow population in regions 2 and 3 in favour of the fast population in region 1. In contrast, inhibition of CCPs formation had a much stronger influence on the binding of NGF to the ACP–TrkA receptor (Fig. 5D,G; Table 1; supplementary material Fig. S4C,D; Table S2), by almost completely inhibiting the populations of regions 2 and 6, and changing the details of the distribution within regions 3 and 4.

Finally, SH-SY5Y cells expressing ACP–TrkA were treated with cytochalasin D (Cyt-D) in order to disrupt the meshwork of actin filaments that are associated with the cytoplasmic face of the plasma membrane and contribute to its structure (supplementary material Fig. S3C). We found that treatment with Cyt-D leads to a significant decrease of the fast-diffusing ACP–TrkA population in resting conditions (Fig. 5E,G; supplementary material Fig. S3E). However, a number of ACP–TrkA receptors remained sensitive to NGF stimulation (Fig. 5F,G; supplementary material Fig. S4E–F), as demonstrated by the higher immobilization of receptors (supplementary material Fig. S3E) and by the higher proportion of receptors residing in areas of low γ and *D*, such as regions 3, 4, 6 in presence of NGF.

Taken together, these results indicate that, whereas K252a and Chlprz treatments impair NGF-induced TrkA dynamic behaviour, Cyt-D administration affects mainly the fast diffusive component, while poorly influencing the NGF-dependent immobile and slow receptor populations. For this reason, the effect of Cyt-D can be best appreciated in the absence of any ligand addition.

Discussion

In this work we explored the lateral mobility of TrkA receptors at the basal membrane of SH-SY5Y cells; in particular, we examined their response to a set of diverse biologically relevant TrkA ligands. We used TIRF microscopy and SPT together with the ACP–TrkA construct, which allows the selective labelling and imaging of single receptor molecules translocated to the plasma membrane (Callegari et al., 2012). We used two different receptor labelling strategies exploiting the versatility of the ACP tag (George et al., 2004; Johnsson et al., 2005). In one case, we biotinylated ACP–TrkA using a CoA-biotin substrate and coupled them to S-Qdots; in the other, we covalently conjugated ACP–TrkA to a CoA derivative of the Atto633 synthetic fluorophore. Tracking the receptor with these two probes allowed us to obtain different and complementary observations on TrkA dynamics. By long-term tracking of the receptor labelled with S-Qdots we observed that TrkA receptors display different dynamic behaviours in resting conditions (Fig. 1C–F) and that the population of each dynamics category

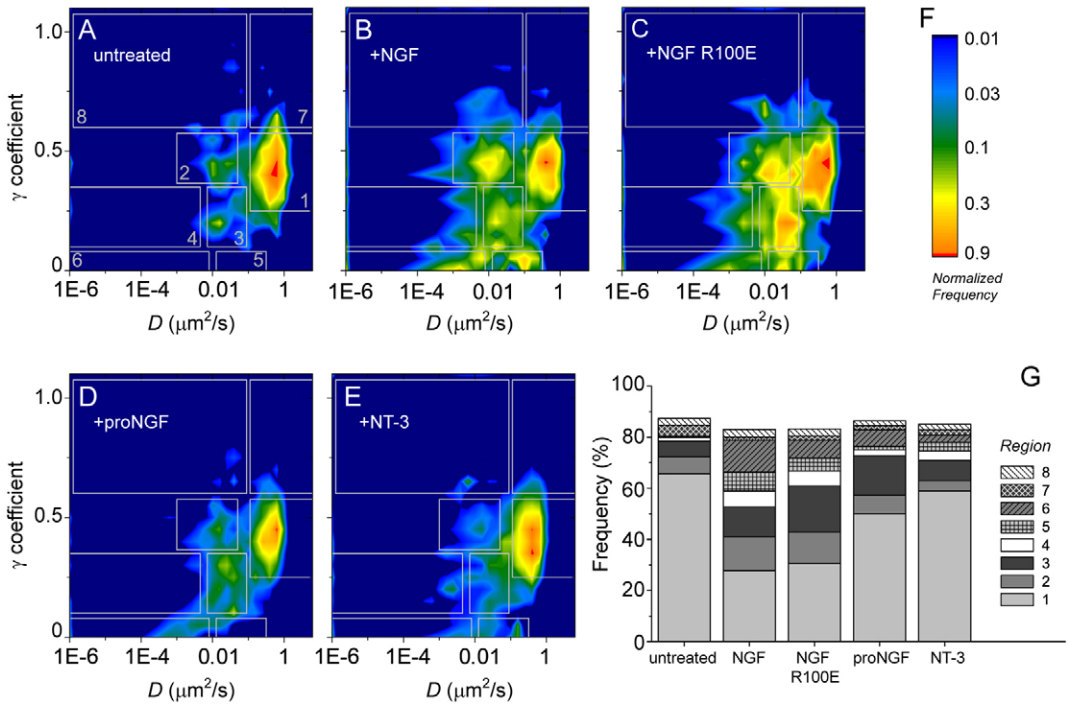

Fig. 4. Effects of ligands on ACP–TrkA dynamics modes. (A–E) Total *D*-γ distributions according to MSS-TAD analysis of ACP–TrkA trajectories in non-stimulated cells (A; $n=677$), and after addition of NGF ($n=909$), NGF R100E ($n=1263$), proNGF ($n=1234$) or NT-3 ($n=1520$; B–E, respectively). Dynamics regions (numbered from 1 to 8 in A) are superimposed on each plot. The diffusion coefficient *D* reflects the short-term diffusivity and the γ factor reflects the long-term trajectory behaviour (γ approximately greater or less than 0.5 for Brownian, drifted, and subdiffusive/confined dynamics, respectively). (F) Logarithmic-scale colour code for the frequency of the total *D*-γ distributions, normalized to 1 at the peak. (G) Frequency percentage of different dynamics modes for ACP–TrkA receptors, as calculated from the integral of the experimental *D*-γ distribution in each numbered region of A–E. These values are reported more fully in supplementary material Table S2.

changes in response to ligand addition and drug treatment (Table 1; Figs 2–5). In addition, by tracking Atto633-ACP–TrkA we could gain insights on the oligomeric status of TrkA, in the absence or presence of NGF (Fig. 2D).

We conclude that in the absence of any stimulus, the diffusion coefficient for TrkA receptors has mostly a bimodal distribution, characterized by two components differing by one order of magnitude (Fig. 2C, top graph). The fast diffusion peak is the most populated: we found TrkA molecules moving with diffusivity higher than 0.1 μm^2/second for more than 70% of the time, and this population corresponds mostly to TrkA monomers (Fig. 2D, black rectangle in the central panel). ACP–TrkA receptors follow (sub)trajectories contributing to the slow diffusion peak for ~1/5 of the time (Fig. 2C, top graph); these stem from receptors in both monomeric and di/oligomeric states (Fig. 2D, white rectangle in the central panel). These receptors are either moving slowly at the cell membrane or undergoing TAD events (Table 1, first row). The remaining trajectories are followed by TrkA molecules that are essentially immobile within a small area of ~0.6 μm diameter (Fig. 1C); these are represented in Fig. 2B by the black histogram and are detected for ~4% of the time (see Table 1).

NGF triggers a reduction of the fast diffusing population, greatly increasing the slow/immobile one (about eightfold), displaying a more restricted confinement (Fig. 2B,C bottom panel; Table 1). Furthermore, a striking shift of the monomer–dimer equilibrium towards the dimeric form can be observed in the fast-diffusing receptor population, whereas receptor clusters containing several – up to eight – receptor molecules make up the slow and immobile populations (Fig. 2D, right panel). These considerations provide a direct demonstration, at the single particle level, of the NGF-induced TrkA dimerization and subsequent clustering at the cell membrane. Notably, our data, obtained from cells displaying low expression of ACP–TrkA, do not support the recent suggestion that NGF only induces dimer phosphorylation of preformed unstimulated TrkA dimers (Shen and Maruyama, 2011).

The observation that ligand binding leads to immobilization and slowing down of lateral mobility was reported for several membrane receptors other than TrkA (Chung et al., 2010; Kasai et al., 2011; Lill et al., 2005; Winter et al., 2011). To date, however, the specific influence of different ligands binding the same type of receptor was poorly investigated, and, to our knowledge, limited to a comparison between agonist and antagonist ligands (Jacquier et al., 2006). Here, we investigated TrkA lateral diffusion induced by the addition and consequent binding of four agonist ligands: NGF, 'painless' mutant NGFR100E, proNGF and NT-3 (Figs 2–4). As schematically depicted in supplementary material Fig. S2, these ligands are known to show different affinity for TrkA, as well as specific modes of receptor activation and/or recruitment of intracellular signalling effectors. Therefore they can be considered full (NGF), partial (NT-3 and proNGF) or biased (NGF R100E) TrkA agonists. Our experiments clearly show a ligand 'fingerprinting' effect on the modifications in TrkA lateral mobility at the single molecule level. Each ligand prompts particular changes in

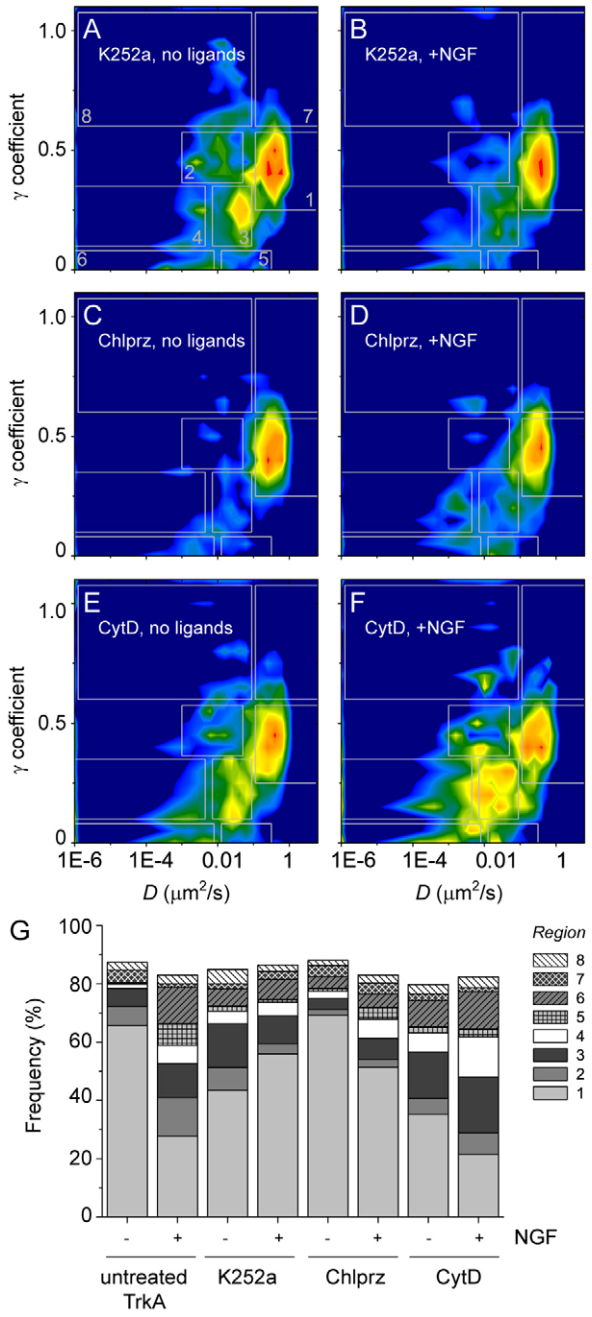

Fig. 5. Effects of drug-induced inhibition of tyrosine-kinase activity, clathrin-coated pit formation and actin meshwork on ACP–TrkA lateral dynamics. (A–F) 2D distribution of γ and *D* for S-Qdot-labelled ACP–TrkA trajectories, as obtained by MSS-TAD analysis (as in Fig. 4A–E; same colour scale as in Fig. 4F). The cells were either unstimulated (left panels) or stimulated (right panels) with NGF, and were treated with K252a (A,B; $n=854$ and 2077, respectively), Chlprz (C,D; $n=1152$ and 1546, respectively) or Cyt-D (E,F; $n=1274$ and 686, respectively). (G) Stack column graph representing the frequency percentage of different dynamics modes for ACP–TrkA receptors under different treatments, calculated as for Fig. 4G (data reported in supplementary material Table S2). The first two stacked-bars, are the same as in Fig. 4G (for comparison).

receptor diffusion, as well as in the fraction and type of immobile trajectories (Fig. 3). The observed heterogeneous responses suggest a complex set of TrkA-receptor dynamics modes upon ligand stimulation. These are only partially described by the diffusion-coefficient distributions and by histograms of the confinement length; therefore, we analysed the 2D distribution of γ and *D* parameters for all TrkA (sub)trajectories (Fig. 4). Moreover, we investigated how TrkA lateral mobility is influenced by drug treatments inhibiting its kinase activity or the early events of clathrin-dependent endocytosis; similarly, we studied the effects of actin meshwork disruption under the plasma membrane (supplementary material Figs S3, S4; Fig. 5). Thus, we were able to quantitatively analyse how ACP–TrkA receptor molecules redistribute among all dynamic and immobile categories (plot regions numbered from 1 to 8 in Fig. 4A and Fig. 5A) as a result of specific ligand addition (Fig. 4) or drug treatment (Fig. 5). The results allowed us to hypothesize a biological significance for almost all of these dynamics regions and to propose a molecular mechanism explaining the heterogeneous responses of TrkA dynamics, as schematically depicted in Fig. 6 and explained in the following.

Region 1 comprises *D* coefficients between 0.1 and 1 μm²/second, and γ values dispersed around 0.5, with a significant tail towards lower values down to 0.25. It is populated by fast almost free-diffusing trajectories, although relatively large regions of confinement (up to several microns) were occasionally detected for them (Table 1, $<L>$ column for fast trajectories). Region 1 is significantly depleted by almost every ligand treatment (Fig. 4); crucially, the higher the ligand affinity for TrkA, the lower is the frequency of trajectories populating region 1 (compare ligand K_d values in supplementary material Fig. S2 with Fig. 4G and to Table 1, column Time% for fast trajectories). We suggest that this region constitutes the 'monomer reservoir' of ACP–TrkA receptors available for ligand capture (it may also include freely diffusing dimers, with no or low interactions with other membrane or cytoplasmic components – see Fig. 6). Differently from region 1, the correlation of ligand-induced changes of the other dynamics regions (2–8) with ligand affinity is not obvious (Table 1). Thus, other factors besides ligand affinity have to be considered to understand the ligand 'fingerprinting' effect.

Region 2 includes trajectories with a low degree of confinement (γ∼0.5 or slightly lower) but displaying a significantly lower diffusion coefficient (10^{-3}–0.5×10^{-1} μm²/second). It becomes highly populated upon NGF addition (Fig. 4B,G), but not when cells are previously treated with the tyrosine kinase inhibitor K252a (Fig. 5B,G; its population falls from ∼13% to 3.5% as reported in supplementary material Table S2), or when the previous treatment with Chlprz causes the disassembly of CCPs (Fig. 5C,D,G).

Region 5 includes receptor trajectories characterized by relatively high short-lag-time diffusion coefficients (*D* between 0.013 and 0.3 μm²/second) and restricted motion (very low γ values). This region is virtually unpopulated when the TrkA receptor is not stimulated (Fig. 4A,G). It becomes highly populated upon NGF addition (Fig. 4B,G), but not if K252a is added to the cell culture prior to NGF (Fig. 5B,G) or if the actin cytoskeleton is disrupted (Fig. 5C,D,G). Interestingly, this region does not appear to be affected dramatically by Chlprz addition prior to NGF treatment (Fig. 5E–G; supplementary material Table S2).

Thus, although TrkA trajectories populating region 5 are affected by ligand-dependent receptor activation by phosphorylation, region 2 is linked to both receptor activation

and CCP formation. We may infer that region 5 includes trajectories involved in the formation of signalling platforms whose motion is hindered most probably by interactions with downstream signalling effectors, possibly linked to actin filaments (Fig. 6). Conversely, region 2 probably corresponds to trajectories of receptors assembling into precursors of signalling endosomes at the plasma membrane (Fig. 6). Interestingly, incubation with NGF R100E causes regions 2 and 5 to be populated to the same extent as in the NGF case (Fig. 4B,C,G); this does not occur for proNGF and NT-3 (Fig. 4D,E,G). This demonstrates that NGF R100E can induce TrkA activation and formation of signalling endosomes similarly to NGF. Thus, the SPT analysis of TrkA trajectories activated by NGF or by the HSAN V-related NGF R100E mutant confirms that the two proteins share a similar binding mechanism to TrkA; identical conclusions have been drawn from different studies (Capsoni et al., 2011). Instead, proNGF and NT-3 induce very different TrkA dynamics. *In vitro* proNGF shows a lower binding affinity to TrkA than NGF (supplementary material Fig. S2) (Paoletti et al., 2009; Covaceuszach et al., 2010); consistently, *in vivo* proNGF induces lower receptor phosphorylation levels than NGF (Fahnestock et al., 2004). We find that proNGF induces a lower number of TrkA receptor trajectories populating regions 5 and 2 (Fig. 4D) that correspond, in our interpretation, to signalling platforms and signalling endosome precursors, respectively. This is consistent with its lower activity through TrkA *in vivo*. The actual contribution of $p75^{NTR}$ co-receptor in modulating proNGF-induced TrkA dynamics remains to be elucidated, given the very low levels of $p75^{NTR}$ in SH-SY5Y cells (supplementary material Fig. S5). It could be that the co-expression of $p75^{NTR}$ enhances proNGF-dependent responses, which could explain the neurotrophic activity displayed by proNGF *in vivo* (Fahnestock et al., 2001). As for NT-3, *in vitro* data show that it binds to TrkA with a binding affinity that is two orders of magnitude lower than NGF (supplementary material Fig. S2). However, increased doses of NT-3 have been shown to activate TrkA and downstream effectors *in vivo* (Harrington et al., 2011; Kuruvilla et al., 2004). Our data show that a 10-fold molar excess of NT-3 over NGF and proNGF is able to activate TrkA, more than proNGF, but less than NGF (region 5 in Fig. 4E,G). However, NT-3 does not cause an enrichment of trajectories that we associate with the assembly of signalling endosomes; this can

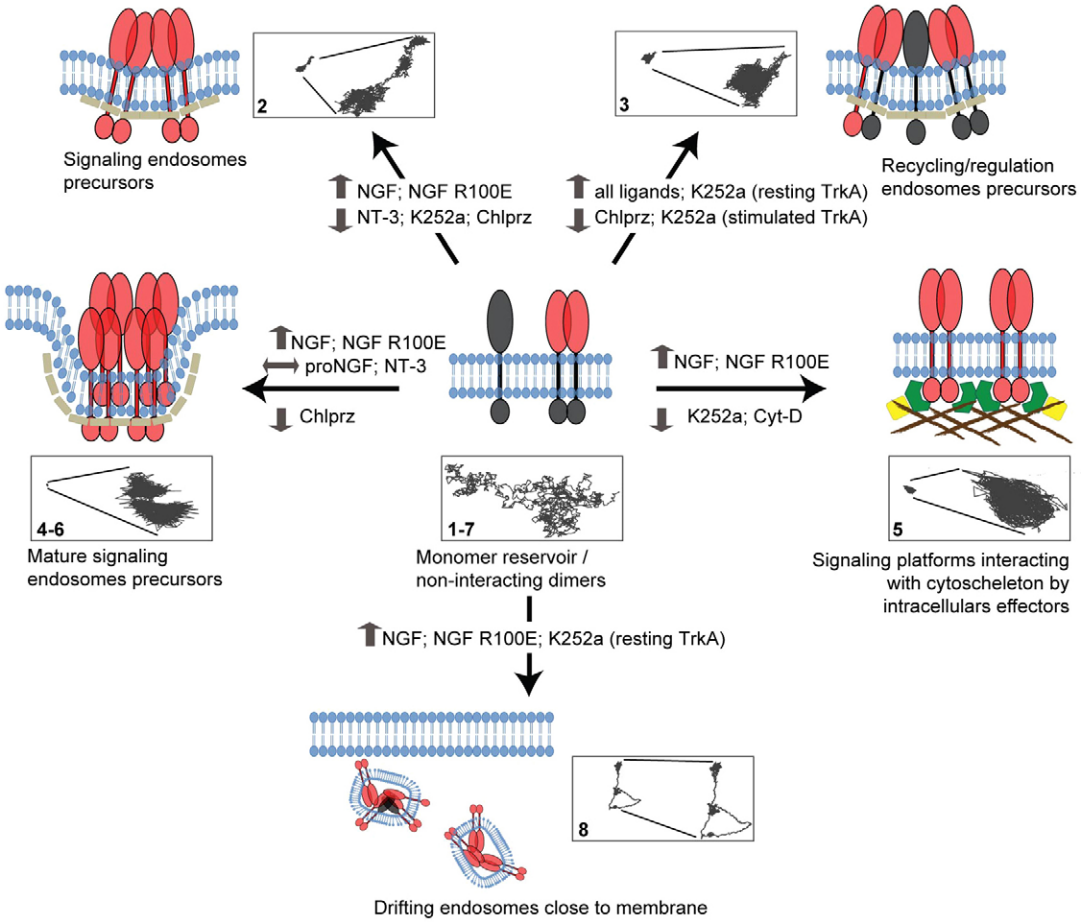

Fig. 6. Model illustrating the fingerprinting effect. This schematic view of possible states of TrkA in its different dynamics modes (numbers refer to the regions in Fig. 4A and Fig. 5A) summarizing our conclusions (see text for further discussion). Insets show a typical trajectory for each dynamics mode, enlarged when necessary to appreciate its details. The population in regions 1 and 7 decreases upon each treatment; changes induced by ligands and/or drug treatments with respect to the unstimulated case are also indicated schematically. Large ellipses represent TrkA extracellular domains (red if bound, grey if unbound), small ellipses the intracellular domains (red if phosphorylated, grey if inactive). The membrane bilayer is in blue; brown rectangles represent clathrin; brown lines represent actin filaments; yellow and green shapes represent possible intracellular effectors.

be deduced from the lack of trajectories in region 2 (but also 4 and 6) and from the lower $<t>$ of TAD events (see Table 1 and supplementary material Table S1), comparable to the case where the formation of CCP (and hence of early endosomes) is inhibited by Chlprz. Failure of NT-3 to induce phosphorylated TrkA internalization (see supplementary material Fig. S2) (Harrington et al., 2011; Kuruvilla et al., 2004) may represent the functional significance of this observed NT-3 signature at the level of receptor dynamics.

Region 3 includes trajectories with a higher degree of confinement than region 2 ($0.1<\gamma<0.35$), but with a slightly higher D (7×10^{-3} to 0.9×10^{-1} μm^2/second). The addition of all TrkA ligands causes an enrichment of trajectories populating region 3, with a similar trend to that of region 2 (compare B–E with A in Fig. 4). The same region is highly populated when the non-stimulated ACP–TrkA receptor is inactivated with K252a (from ~6% in resting conditions to 15% upon K252a administration; supplementary material Table S2). Moreover this region, similarly to region 2, is sensitive to Chlprz treatment, and is highly depopulated by this drug either in the presence or absence of NGF (Fig. 5E–G). These data suggest that region 3 is populated mainly by receptors primed for constitutive recycling, internalization, degradation or a feedback loop regulating the functional response to ligands (Fig. 6). It was quite surprising to find out that NGF R100E populates region 3 slightly more than NGF (Fig. 4B,C,G). NGF and NGF R100E indeed share a similar activation of TrkA receptor; however, these growth factors demonstrate a different extent of PLCγ pathway activation (see supplementary material Fig. S2) (Capsoni et al., 2011). Clearly, this functional difference corresponds to the subtle modification of the D-γ distribution reported in Fig. 4C. The precise reasons why NGF R100E addition increases the number of recycling receptors compared with NGF remains to be explored. Still, our SPT analysis method provides a very sensitive measure of TrkA receptor activation, and makes it possible to detect minimal differences between various ligands.

Regions 4 and 6 include the slowest-diffusing trajectories down to very low γ values corresponding to the immobile ones; these are reported in Table 1 and their confinement length was analysed (Fig. 2B; Fig. 3A–C; supplementary material Fig. S3A,C,E). Given the susceptibility of these trajectories to Chlprz treatment (Fig. 5C,D,G), they probably correspond to ACP–TrkA multimers inside more mature signalling endosomes ready to be actively internalized (Fig. 6). Indeed, these regions are mostly populated when incubating TrkA with NGF and NGF R100E ligands (Fig. 4B,C), with the two ligands leading to the highest TrkA internalization, but not with proNGF and NT-3 (Fig. 4D,E).

Finally, regions 7 and 8 include drifted trajectories with $\gamma>0.5$ and can be fast (region 7) or slow (region 8). The fast drifted trajectories are reduced by ligand addition, similar to the trajectories in region 1 (supplementary material Table S2), and can therefore be considered as the high-γ tail of the fast freely diffusing population. As for the slow drifted population of region 8, it is very poorly populated in almost all considered conditions. These trajectories might stem from ACP–TrkA receptor molecules localized within internalized sub-membrane vesicles (Fig. 6), which are still detectable because of the high fluorescence quantum yield of Qdots and the higher number of Qdots present within such vesicles.

The actin meshwork disruption caused by Cyt-D treatment mostly induces a higher population in region 3, which we interpret as the group of inactive receptors that are constitutively recycled and possibly degraded. Moreover, we observed a small shift towards lower values of the characteristic D value of the faster population. These data are apparently not in agreement with the *fence-and-pickets* model (Kusumi et al., 2005): according to that model, when inducing a partial actin depolymerization by short drug treatment, there are less actin filaments barriers so that an increase in receptor diffusion can be observed (Suzuki et al., 2007), eventually determining an enhanced availability of receptor molecules for signalling (Treanor et al., 2010). However, we should note that different receptors may have distinct sensitivities to disruption of the sub-membrane actin meshwork; moreover, the actin disruption performed in our experiments was not partial (see Materials and Methods and supplementary material Fig. S3C). It is in principle possible that after prolonged drug treatment the TrkA 'monomers reservoir', normally maintained by a functional actin meshwork, undergoes processes such as constitutive internalization, while still being available for signalling events upon ligand treatments (Fig. 5E,F). Indeed, we do see an increased fraction of either confined or immobile receptors upon NGF administration, in the presence of Cyt-D (Fig. 5F,G; supplementary material Fig. S4E–F; Table 1), although the confinement and diffusivity features of signalling platforms (normally populating region 5) and signalling endosomes precursors (normally within regions 2, 4, 6) are here completely shifted by the drug treatment.

From a general perspective, the main conclusion from these experiments is that receptor dynamics in the plasma membrane carries a signature tracing back to its specific activation event. TrkA lateral mobility was shown to be a sensitive predictor of full, partial, or biased agonists that bind to the receptor. The ligand signature results from a different binding affinity of a given ligand for the receptor, from the specific intracellular effectors recruited in the signalling platforms and/or from the formation of endosome precursors. The second conclusion that we can draw from these experiments is that the specific biological outcomes induced by different ligands binding to the same receptor can be reliably traced back to the earliest events of receptor activation, namely the initial receptor membrane movements triggered upon binding. Indeed, different TrkA agonists, all binding TrkA specifically and activating, through TrkA, different cellular processes, trigger distinct trajectory patterns of TrkA molecules at the cell membrane.

How the ligand signature of TrkA dynamics is influenced by its co-receptor $p75^{NTR}$ is an important question that remains to be addressed. Answering such a question requires the ability to perform SPT of the two receptors simultaneously. Another open issue is the generalization of the dynamic fingerprint concept to other receptors: hypothetically, there may be a causal correlation between dynamic fingerprints and signalling pathways.

Materials and Methods

Cell surface labelling of ACP–TrkA expressed in living SH-SY5Y cells

SH-SY5Y cells were transfected with ACP–TrkA construct (Callegari et al., 2012). Between 3 and 5 hours after transfection, cells were trypsinized and transferred into Willco-dish® glass-bottom dishes. Cells were allowed to attach overnight, then serum starved for 2 hours, and incubated for 30 minutes at 37℃ in DMEM-F12 with 0.5% BSA, containing 1.0 μM of Sfp synthase (New England Biolabs), 10 mM $MgCl_2$ and variable amounts of coenzyme A derivative depending on the

experiment. For the labelling with S-Qdots for single-molecule experiments, 5 µM biotin-CoA was used, then cells were washed twice in PBS before incubation for 2 minutes at room temperature with 2 nM S-Qdot (Qdot® 655 streptavidin conjugate; Invitrogen) in borate buffer pH 8.3, 0.5% BSA and 215 mM sucrose (Bannai et al., 2007). These conditions ensured a minimal non-specific adhesion of S-Qdots to the glass surface. To achieve a 'bulk' labelling of ACP–TrkA construct at the plasma membrane (Fig. 1A), 20 nM S-Qdot was incubated for 15 minutes, then cells were fixed, mounted in DAPI-containing VectaShield and imaged using an Olympus FV1000 confocal microscope with a 40× objective and the 488 nm argon laser line to image both the GFP and the S-Qdot655 channels and a 405 nm laser for DAPI excitation. For labelling with Atto633 fluorophore, 5 nM CoA–Atto633 conjugate was used as a substrate in the reaction mix to yield complete receptor labelling. Cells were imaged in imaging medium (20 mM HEPES, 6.6 mM D-glucose, 2 mM L-glutamine, 1 mM sodium pyruvate and 0.5% B-27 supplement in MEM medium) after extensive washing (8–10 times with PBS). Notably, no significant differences in receptor immobile populations and in D distributions were detected when labelling the receptor with either monovalent Atto633–CoA fluorophore or multivalent S-Qdots. This observation supports the idea that potential S-Qdots-mediated receptor crosslinking is minimized under our experimental conditions (low Qdot concentration, use of BSA in the labelling reaction and analysis of cells displaying low-level expression of receptor).

Synthesis of biotin-maleimide

Biotin (10 mg) dissolved in DMF (250 µl), NHS (1.1 eq), 2-aminoethylmaleimide (1.1 eq) and EDC (1.2 eq) were mixed, and the solution stirred for 4 hours at 25℃. The product was purified by semi-preparative RP-HPLC.

Synthesis of CoA-biotin and CoA-Atto633

Coenzyme A (10 nmol), dissolved in DMF (2 µl), was mixed with the appropriate maleimido derivative (20 nmol) in DMF (10 mM). The solution was stirred at 35℃ for 4 hours. The product was purified by RP-HPLC (column: Phenomenex Fusion 150×4.6. Solvents: ammonium formate 5 mM/acetonitrile).

Ligand treatments

Transfected SH-SY5Y cells were treated with different ligands: native mouse NGF (Alomone Labs, 125 ng/ml), recombinant human pro-NGF (300 ng/ml), recombinant human NGF R100E (125 ng/ml) and recombinant human NT-3 (Alomone Labs, 1000 ng/ml). Equimolar doses of NGF, NGF R100E and proNGF were used, and NT-3 was administered in a 10-fold molar excess over NGF, as reported (Harrington et al., 2011; Kuruvilla et al., 2004). Recombinant proNGF and NGF R100E mutant were expressed in *E. coli* and purified as described (Covaceuszach et al., 2010). All ligands were added as two-times concentrated, pre-warmed (37℃) solutions to an equal volume of imaging medium directly into Willco-dish® glass-bottomed chambers used for microscopy. Cells were always imaged for a maximum of 15 minutes upon ligand addition.

Drug treatments

For the inhibition of TrkA kinase activity, ACP–TrkA-expressing SH-SY5Y cells were treated overnight with 200 nM K252a (Sigma-Aldrich) before the labelling reaction. To block the endocytosis machinery, transfected cells were exposed to 25 µM Chlprz (Sigma-Aldrich) during the ACP-labelling reaction. In order to disrupt the actin meshwork at the plasma membrane, transfected cells were treated with 1 µM Cyt-D (Sigma-Aldrich) for 2 hours, during the serum starvation preceding the cell surface labelling of ACP–TrkA. Each drug was also added to the imaging medium, keeping the Cyt-D concentration unaltered, while K252a was lowered to 100 nM in the labelling reaction and imaging medium and Chlprz was increased to 50 µM in the imaging medium.

Microscope image acquisition

Cells prepared as described above were immediately imaged at 37℃, 5% CO_2 with a Leica DM6000 microscope equipped with Leica TIRF-AM module, incubator chamber, electron multiplying charge-coupled-device camera (ImagEM C9100-13, Hamamatsu), and 100× oil immersion objective (NA 1.47). TIRF time series were acquired on a ROI with constant size of 144×152 pixels (32.7×34.5 µm) within the basal membrane of each cell, using the 488 nm laser line with a Qdot655/10 emission filter, or the 632 nm laser line with a Cy5 Leica1152303 emission filter, and penetration depth set at 90 nm. The integration time per frame was 21 mseconds and typical time series lasted 3000 frames. The lag time between two consecutive frames was minimized to the integration time (21 mseconds) by using the overlapping mode of the CCD camera with the reduced ROI. Cells with low density of Qdots where chosen to calculate trajectories.

Data analysis

Detection and localization of S-Qdots conjugated to biotinylated ACP–TrkA or CoA-Atto633-labeled ACP–TrkA, linking and merging of the trajectories was done using Imaris software (Bitplane Scientific Software). We found the following software parameters to be optimal to overcome splitting caused by Qdot blinking: estimated spot diameter 0.8 µm, Brownian motion algorithm, max spot distance 1 µm, max gap size 30 frames. Visual inspection of the resulting trajectories and their manual editing was performed in case of linking mistakes by the algorithm. Spots of fluorophores non-specifically adhered to the glass outside the cell were discarded by considering the merge of the TIRF over the DIC image. Qdots non-specifically adhered to the glass under the basal membrane of the investigated cells were found to be negligible or anyway not interfering with TrkA trajectories analysis (supplementary material Fig. S6).

Further analyses on the trajectories were carried out almost automatically using codes written in MatLab, which performed the analyses described in supplementary material Fig. S7 and summarized in the following. The trajectories acquired in the case of CoA–Atto633-labelled ACP–TrkA were relatively short and very numerous: they were analysed all together, only considering their average short-lag-time diffusion coefficient $D\pm$s.e. as deduced from the initial angular coefficient of the mean square displacement (MSD) (Callegari et al., 2012), and considering the average intensity$\pm$s.d. on whole trajectories (Fig. 2D). In the case of Qdot-labelled receptors, we first used the moment scaling spectrum (MSS) analysis (Ewers et al., 2005) in order to separate self-similar from multimodal trajectories; the latter were analysed using an algorithm for the detection of non-random transient confinement zones (Simson et al, 1995), similar to the stimulation-induced transient arrest of lateral diffusion (STALL) method (Suzuki et al., 2007). Our algorithm is here referred to as TAD (transient arrest of diffusion) because such events were observed also for the TrkA receptor in the absence of any stimulation. For all trajectories and subtrajectories (determined by TAD analysis) we calculated the MSD, the MSS and the average spot intensity $<I>\pm$s.d., also checking if the diffusing subtrajectories and the confinement events predicted by TAD were correct. The confinement length parameter L was calculated using the MSD fit for 'confined' trajectories only if those were long enough to explore the confinement area substantially (Callegari et al., 2012); the sub/super-diffusive coefficient γ with its uncertainty was determined by a fit of the MSS. A schematic view of this analysis and more details about it can be found in supplementary material Fig. S7 and its caption.

All 1D or 2D distributions or histograms reported here were evaluated weighting each (sub)trajectory by the number of spots composing it and, except where stated differently, their integrals were normalized to 1. Except for L, the uncertainties of the parameters were considered by summing 1D or 2D Gaussians for computing the experimental distributions. A colour code in logarithmic scale, with the maximum normalized to 1, allowed visualization of the 2D distributions.

Acknowledgements

The authors thank Fulvio Bonsignore for investigating endogenous levels of $p75^{NTR}$ in PC12 and SH-SY5Y cells; Alessandro Duci for providing the starting material for coding the analysis algorithms; Francesca Paoletti, Doriano Lamba and Simona Capsoni for helpful discussions and critical revisions of the paper.

Author contributions

L.M. and A.C. performed experiments; S.L. set up and supervized microscopy experiments, and developed and coded the algorithms for data analysis; L.M., A.C., S.L., F.B. and A.C. designed and analyzed experiments, and wrote the manuscript; G.S. synthesized CoA-conjugated substrates for ACP labelling; A.V. prepared and purified recombinant NGF R100E mutant and proNGF proteins.

Funding

This work was supported by Futuro in Ricerca B [grant numbers RBAP11X42L_003 to F.B., RBAP10L8TY to A.C.]; and PRIN [grant number 2009XPTWM2 to S.L.].

Supplementary material available online at
http://jcs.biologists.org/lookup/suppl/doi:10.1242/jcs.129916/-/DC1

References

Bannai, H., Lévi, S., Schweizer, C., Dahan, M. and Triller, A. (2007). Imaging the lateral diffusion of membrane molecules with quantum dots. *Nat. Protoc.* **1**, 2628-2634.

Callegari, A., Luin, S., Marchetti, L., Duci, A., Cattaneo, A. and Beltram, F. (2012). Single particle tracking of acyl carrier protein (ACP)-tagged TrkA receptors in PC12nnr5 cells. *J. Neurosci. Methods* **204**, 82-86.

Capsoni, S., Covaceuszach, S., Marinelli, S., Ceci, M., Bernardo, A., Minghetti, L., Ugolini, G., Pavone, F. and Cattaneo, A. (2011). Taking pain out of NGF: a

"painless" NGF mutant, linked to hereditary sensory autonomic neuropathy type V, with full neurotrophic activity. *PLoS ONE* **6**, e17321.

Chung, I., Akita, R., Vandlen, R., Toomre, D., Schlessinger, J. and Mellman, I. (2010). Spatial control of EGF receptor activation by reversible dimerization on living cells. *Nature* **464**, 783-787.

Covaceuszach, S., Capsoni, S., Marinelli, S., Pavone, F., Ceci, M., Ugolini, G., Vignone, D., Amato, G., Paoletti, F., Lamba, D. et al. (2010). In vitro receptor binding properties of a "painless" NGF mutein, linked to hereditary sensory autonomic neuropathy type V. *Biochem. Biophys. Res. Commun.* **391**, 824-829.

Cui, B., Wu, C., Chen, L., Ramirez, A., Bearer, E. L., Li, W. P., Mobley, W. C. and Chu, S. (2007). One at a time, live tracking of NGF axonal transport using quantum dots. *Proc. Natl. Acad. Sci. USA* **104**, 13666-13671.

D'Onofrio, M., Paoletti, F., Arisi, I., Brandi, R., Malerba, F., Fasulo, L. and Cattaneo, A. (2011). NGF and proNGF regulate functionally distinct mRNAs in PC12 cells: an early gene expression profiling. *PLoS ONE* **6**, e20839.

Echarte, M. M., Bruno, L., Arndt-Jovin, D. J., Jovin, T. M. and Pietrasanta, L. I. (2007). Quantitative single particle tracking of NGF-receptor complexes: transport is bidirectional but biased by longer retrograde run lengths. *FEBS Lett.* **581**, 2905-2913.

Einarsdottir, E., Carlsson, A., Minde, J., Toolanen, G., Svensson, O., Solders, G., Holmgren, G., Holmberg, D. and Holmberg, M. (2004). A mutation in the nerve growth factor beta gene (NGFB) causes loss of pain perception. *Hum. Mol. Genet.* **13**, 799-805.

Ewers, H., Smith, A. E., Sbalzarini, I. F., Lilie, H., Koumoutsakos, P. and Helenius, A. (2005). Single-particle tracking of murine polyoma virus-like particles on live cells and artificial membranes. *Proc. Natl. Acad. Sci. USA* **102**, 15110-15115.

Fahnestock, M., Michalski, B., Xu, B. and Coughlin, M. D. (2001). The precursor pro-nerve growth factor is the predominant form of nerve growth factor in brain and is increased in Alzheimer's disease. *Mol. Cell. Neurosci.* **18**, 210-220.

Fahnestock, M., Yu, G., Michalski, B., Mathew, S., Colquhoun, A., Ross, G. M. and Coughlin, M. D. (2004). The nerve growth factor precursor proNGF exhibits neurotrophic activity but is less active than mature nerve growth factor. *J. Neurochem.* **89**, 581-592.

George, N., Pick, H., Vogel, H., Johnsson, N. and Johnsson, K. (2004). Specific labeling of cell surface proteins with chemically diverse compounds. *J. Am. Chem. Soc.* **126**, 8896-8897.

Harrington, A. W., St Hillaire, C., Zweifel, L. S., Glebova, N. O., Philippidou, P., Halegoua, S. and Ginty, D. D. (2011). Recruitment of actin modifiers to TrkA endosomes governs retrograde NGF signaling and survival. *Cell* **146**, 421-434.

Jacquier, V., Prummer, M., Segura, J. M., Pick, H. and Vogel, H. (2006). Visualizing odorant receptor trafficking in living cells down to the single-molecule level. *Proc. Natl. Acad. Sci. USA* **103**, 14325-14330.

Jaqaman, K., Kuwata, H., Touret, N., Collins, R., Trimble, W. S., Danuser, G. and Grinstein, S. (2011). Cytoskeletal control of CD36 diffusion promotes its receptor and signaling function. *Cell* **146**, 593-606.

Johnsson, N., George, N. and Johnsson, K. (2005). Protein chemistry on the surface of living cells. *ChemBioChem* **6**, 47-52.

Jullien, J., Guili, V., Derrington, E. A., Darlix, J. L., Reichardt, L. F. and Rudkin, B. B. (2003). Trafficking of TrkA-green fluorescent protein chimerae during nerve growth factor-induced differentiation. *J. Biol. Chem.* **278**, 8706-8716.

Kasai, R. S., Suzuki, K. G., Prossnitz, E. R., Koyama-Honda, I., Nakada, C., Fujiwara, T. K. and Kusumi, A. (2011). Full characterization of GPCR monomer-dimer dynamic equilibrium by single molecule imaging. *J. Cell Biol.* **192**, 463-480.

Klein, R., Jing, S. Q., Nanduri, V., O'Rourke, E. and Barbacid, M. (1991). The trk proto-oncogene encodes a receptor for nerve growth factor. *Cell* **65**, 189-197.

Kuruvilla, R., Zweifel, L. S., Glebova, N. O., Lonze, B. E., Valdez, G., Ye, H. and Ginty, D. D. (2004). A neurotrophin signaling cascade coordinates sympathetic neuron development through differential control of TrkA trafficking and retrograde signaling. *Cell* **118**, 243-255.

Kusumi, A., Nakada, C., Ritchie, K., Murase, K., Suzuki, K., Murakoshi, H., Kasai, R. S., Kondo, J. and Fujiwara, T. (2005). Paradigm shift of the plasma membrane concept from the two-dimensional continuum fluid to the partitioned fluid: high-speed single-molecule tracking of membrane molecules. *Annu. Rev. Biophys. Biomol. Struct.* **34**, 351-378.

Lee, R., Kermani, P., Teng, K. K. and Hempstead, B. L. (2001). Regulation of cell survival by secreted proneurotrophins. *Science* **294**, 1945-1948.

Levi-Montalcini, R. (1987). The nerve growth factor 35 years later. *Science* **237**, 1154-1162.

Lill, Y., Martinez, K. L., Lill, M. A., Meyer, B. H., Vogel, H. and Hecht, B. (2005). Kinetics of the initial steps of G protein-coupled receptor-mediated cellular signaling revealed by single-molecule imaging. *ChemPhysChem* **6**, 1633-1640.

Nomura, M., Nagai, T., Harada, Y. and Tani, T. (2011). Facilitated intracellular transport of TrkA by an interaction with nerve growth factor. *Dev. Neurobiol.* **71**, 634-649.

Paoletti, F., Covaceuszach, S., Konarev, P. V., Gonfloni, S., Malerba, F., Schwarz, E., Svergun, D. I., Cattaneo, A. and Lamba, D. (2009). Intrinsic structural disorder of mouse proNGF. *Proteins* **75**, 990-1009.

Rajan, S. S., Liu, H. Y. and Vu, T. Q. (2008). Ligand-bound quantum dot probes for studying the molecular scale dynamics of receptor endocytic trafficking in live cells. *ACS Nano* **2**, 1153-1166.

Reichardt, L. F. (2006). Neurotrophin-regulated signalling pathways. *Philos. Trans. R. Soc. B* **361**, 1545-1564.

Resch-Genger, U., Grabolle, M., Cavaliere-Jaricot, S., Nitschke, R. and Nann, T. (2008). Quantum dots versus organic dyes as fluorescent labels. *Nat. Methods* **5**, 763-775.

Shen, J. and Maruyama, I. N. (2011). Nerve growth factor receptor TrkA exists as a preformed, yet inactive, dimer in living cells. *FEBS Lett.* **585**, 295-299.

Shibata, S. C., Hibino, K., Mashimo, T., Yanagida, T. and Sako, Y. (2006). Formation of signal transduction complexes during immobile phase of NGFR movements. *Biochem. Biophys. Res. Commun.* **342**, 316-322.

Simson, R., Sheets, E. D. and Jacobson, K. (1995). Detection of temporary lateral confinement of membrane proteins using single-particle tracking analysis. *Biophys. J.* **69**, 989-993.

Sundara Rajan, S. and Vu, T. Q. (2006). Quantum dots monitor TrkA receptor dynamics in the interior of neural PC12 cells. *Nano Lett.* **6**, 2049-2059.

Suzuki, K. G., Fujiwara, T. K., Edidin, M. and Kusumi, A. (2007). Dynamic recruitment of phospholipase C gamma at transiently immobilized GPI-anchored receptor clusters induces IP3-Ca2+ signaling: single-molecule tracking study 2. *J. Cell Biol.* **177**, 731-742.

Tani, T., Miyamoto, Y., Fujimori, K. E., Taguchi, T., Yanagida, T., Sako, Y. and Harada, Y. (2005). Trafficking of a ligand-receptor complex on the growth cones as an essential step for the uptake of nerve growth factor at the distal end of the axon: a single-molecule analysis. *J. Neurosci.* **25**, 2181-2191.

Treanor, B., Depoil, D., Gonzalez-Granja, A., Barral, P., Weber, M., Dushek, O., Bruckbauer, A. and Batista, F. D. (2010). The membrane skeleton controls diffusion dynamics and signaling through the B cell receptor. *Immunity* **32**, 187-199.

Winter, P. W., Van Orden, A. K., Roess, D. A. and Barisas, B. G. (2012). Actin-dependent clustering of insulin receptors in membrane microdomains. *Biochim. Biophys. Acta* **1818**, 467-473.

Supplementary Figures

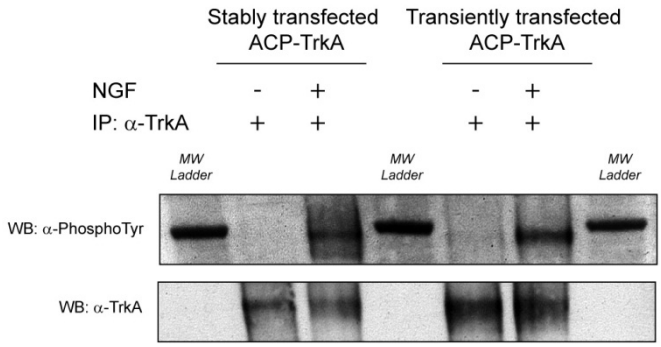

Supplementary Figure 1: ACP-TrkA phosphorylation: effects of NGF and overexpression. SH-SY5Y cells were transfected, either transiently or stably, with pIRES-ACP-TRKA/AcGFP1 construct (Callegari et al., 2012). The phosphorylation of ACP-TrkA in the two cases was monitored by immunoprecipitation (IP) with anti-TrkA (sc-11, Santa Cruz Biotechnology) from 500 µg total cell extracts, also after NGF treatment (100 ng/ml) for 10 minutes at 37°C prior to cell lysis, and subsequent WB against phosphotyrosine (05-321, Millipore, 1:1000) and TrkA (06-574, Millipore, 1:1000). The ACP-TrkA is mainly phosphorylated upon NGF administration, but transient overexpression can lead to some background phosphorylation.

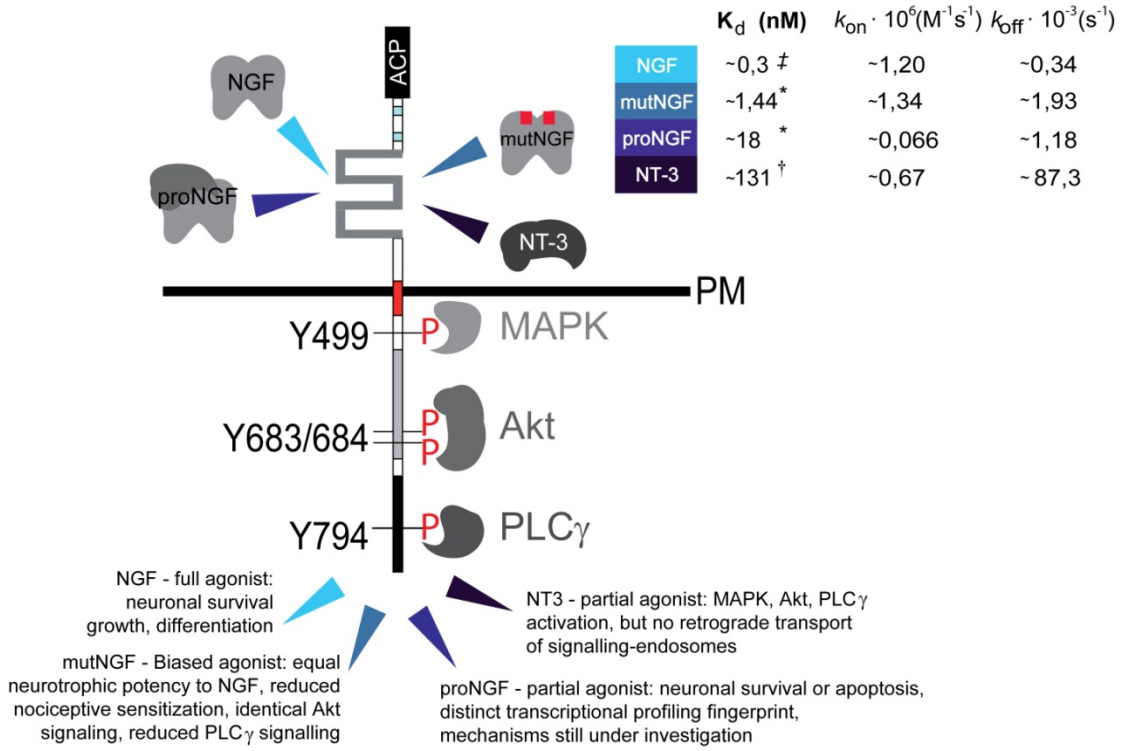

Supplementary Figure 2: TrkA ligands affinity and biological outcomes. Schematic picture of the ACP-TrkA construct, the studied ligands and intracellular effectors. Nerve Growth Factor (NGF; full agonist), NGF R100E mutant (mutNGF; biased agonist), the NGF pro-neurotrophin (proNGF; partial agonist) and the Neurotrophin-3 (NT-3; partial agonist) all bind to the extracellular domain of TrkA receptor but with different affinity (K_d; see the color-coded arrowheads referring directly to K_d values). Evoked physiological responses are summarized for each binding ligand described. Noteworthy, some mechanisms triggering a specific cell response need to be elucidated (*e.g.* proNGF-dependent signaling pathway). *From: Covaceuszach et al, BBRC (2010), 391(1), pp.824-829 † From: Ivanisevic L. et al, J. Biol. Chem. (2007), 282(23), pp.16754-16763 ‡ From: Paoletti F. et al, Proteins (2009), 75(4), pp. 990-1009.

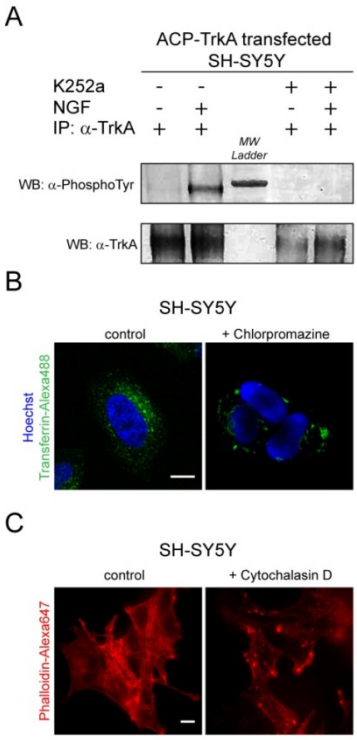

Supplementary Figure 3: Control of drug-induced inhibition of tyrosine-kinase activity, clathrin-coated pits (CCPs) formation and actin meshwork disruption. A) NGF-induced phosphorylation of ACP-TrkA was monitored by IP of TrkA from total cell extracts of transfected SH-SY5Y cells (untreated or treated with K252a kinase inhibitor) and subsequent WB against phosphotyrosine. The ACP-TrkA is phosphorylated upon NGF administration (first two lanes), but gets insensitive to NGF administration after overnight treatment of the cells with K252a (last two lanes). **B)** SH-SY5Y cells were serum-starved for 2 hours, then incubated for 30 minutes with 25 µM chlorpromazine (Chlprz), before 15 minutes incubation with 0.3 µM transferrin-Alexa488 (Invitrogen) in starvation medium, 1% BSA and 25 µM Chlprz. Cells were washed three times with PBS and immediately imaged at the confocal microscope in complete medium supplemented with 50 µM Chlprz and Hoechst. Cells treated with Chlprz display inhibited internalization, via clathrin-coated pits (CPPs) dependent endocytosis, of transferrin-Alexa488 (right panels), when compared to untreated cells (left panels). **C)** SH-SY5Y cells were serum-starved for 2 hours either in the presence or in the absence of 1 µM cytochalasin D (Cyt-D). They were washed twice with PBS, fixed with 4% paraformaldehyde and stained with Phalloidin-Alexa647 (Invitrogen). Cells were mounted in DAPI-containing Vectashield and imaged at the TIRF microscope. TIRF images show Cyt-D-induced disruption of actin meshwork in Cyt-D treated SH-SY5Y cells (right panels) compared to untreated cells (left panel); the drug induces a spot-like pattern of the actin-meshwork.

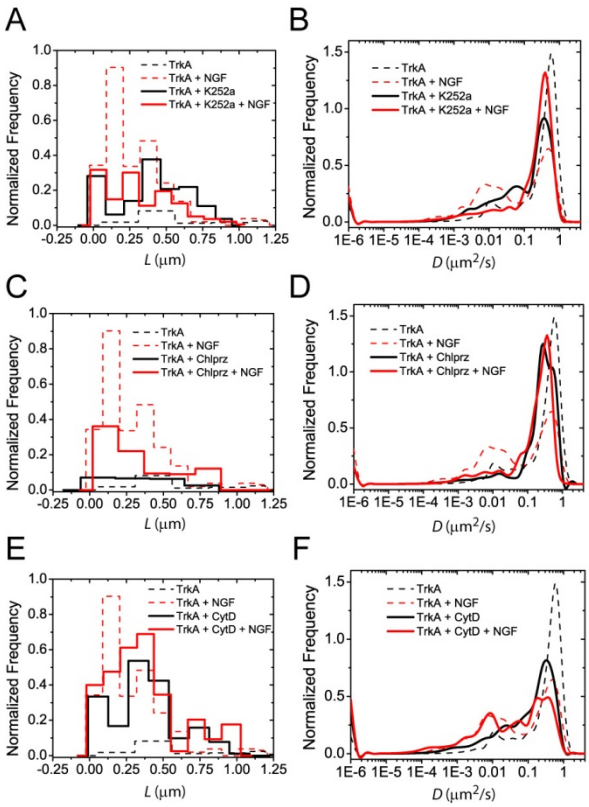

Supplementary Figure 4: Effects of drug-induced inhibition of tyrosine-kinase activity, clathrin-coated pits (CCPs) formation and actin meshwork on ACP-TrkA diffusivity. A-C-E) Distributions of the confinement length (*L*) for immobile trajectories of S-Qdots labelled ACP-TrkA receptors in the absence (black solid curves) or presence (red solid curves) of NGF, after treatment with K252a (panel A), chlorpromazine (Chlprz; panel C), Cytochalasin D (CytD; panel E). The dashed curves reported in each graph correspond to the confinement length distribution histograms of ACP-TrkA immobile receptors in the absence of drugs (see Figure 2B). The areas under the curves are normalized to the fractions of spots assigned to immobile trajectories for each treatment. **B-D-F)** Diffusion coefficient (*D*) distribution for S-Qdots-labelled ACP-TrkA mobile receptors in the absence (black solid curves) or presence (red solid curves) of NGF, after treatment with K252a (panel B), chlorpromazine (Chlprz; panel D), Cytochalasin D (CytD; panel F). The dashed curves reported in each graph (same data of Figure 2C) are reported here for comparison to the untreated cases. The average diffusivity distribution has been calculated considering all trajectories but the immobile ones. The areas under the distributions are normalized to the relative weight of these trajectories, as in Figures 2C and 3D–F

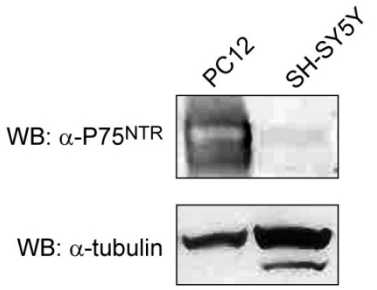

Supplementary Figure 5: Endogenous expression of p75^{NTR} in PC12 and SH-SY5Y cells. Equal amounts (~50 µg) of total cell extracts from PC12 (left lane) and SH-SY5Y (right lane) were subjected to WB using anti- p75^{NTR} (07-476, Millipore, 1:1000) and anti-tubulin (Clone B-512, Sigma, 1:2000) primary antibodies. The expression of P75^{NTR} is so higher in PC12 than in SH-SY5Y that the corresponding band results over-exposed in the PC12 lane, while it is barely visible in the SH-SY5Y lane.

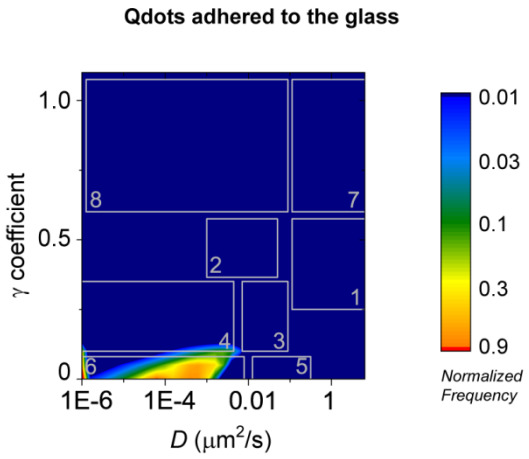

Supplementary Figure 6: Total *D*-γ distributions according to MSS-TAD analysis of S-Qdots non-specifically adhered to the glass surface. Trajectories coming from the tracking of 11 S-QDots on a portion of the glass surface of a Willco Petri dish devoid of cells were subjected to the same MSS-TAD analysis as used for ACP-TrkA trajectories (see Fig. S7). Dynamics regions (numbered from 1 to 8) are superimposed on the plot. The logarithmic scale colour code represents the frequency of the total *D*-γ distributions, normalized to 1 at the peak (in this case barely visible as it falls at γ around 0). The graph shows that trajectories coming from glass-adhered S-Qdots populate region 6 only. This region is not populated by ACP-TrkA trajectories when the receptor is in resting conditions (Fig. 4A). These data indicate that immobile trajectories detected for ACP-TrkA depend on the biological effect specifically raised by some ligands (see e.g. Fig. 4B-C) and/or drug treatments (see e.g. Fig. 5E-F) and are not just immobile Qdots non-specifically bound to the glass under the cell.

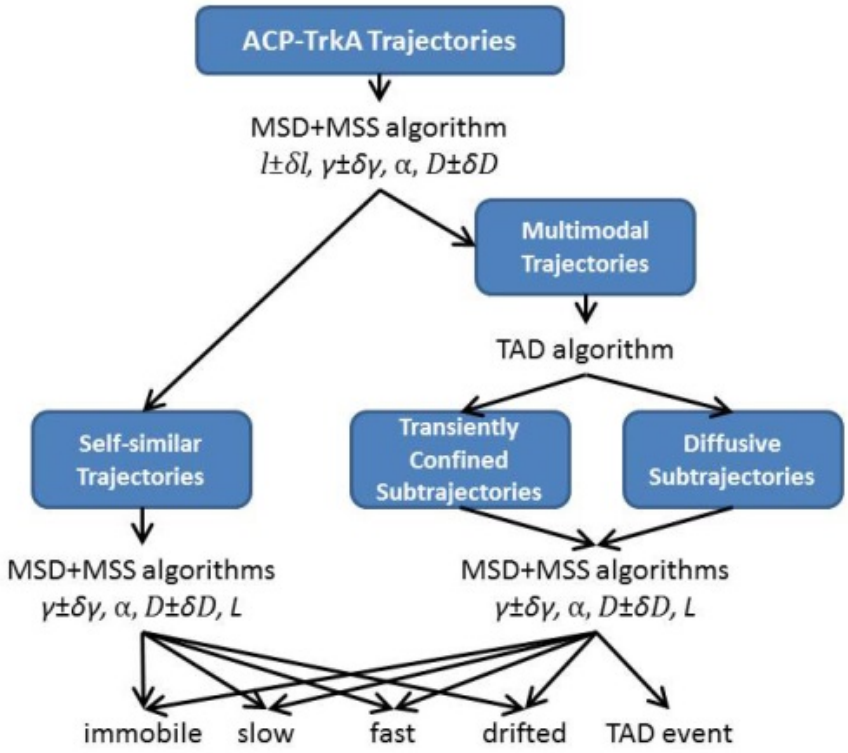

Supplementary Figure 7: Simplified flowchart for the analysis of QDots-labelled ACP-TrkA trajectories. Moment scaling spectrum (MSS) analysis consists in calculating for each trajectory the moments $\mu_\nu(t)$ of order ν=1…6 as a function of the lag-time t (i.e. the average ν^{th} power of the displacement after t); note that $\mu_2(t)$ is the mean square displacement (MSD). $\mu_\nu(t)$ are then fitted with a function of the form $\mu_\nu(t)=\eta_\nu\sigma^\nu+4D_\nu\cdot t^{\gamma\nu}$, as in (Ewers et al., 2005), but considering also the localization precision σ ($\eta_\nu=2^{\nu-1}\Gamma[(\nu+1)/2]$); from this analysis we used the anomalous diffusion parameter $\alpha=2\gamma_2$, the angular coefficient $l\pm\delta l$ for the linear fit in a log-log plot of ν versus γ_ν (to evaluate the self-similarity of a trajectory), and $\gamma\pm\delta\gamma$ from the linear fit $\gamma_\nu = \gamma\nu$. The MSD curve was used to calculate the short-lag-time average diffusion coefficient D (and its s.e. δD) from its first two points, and the confinement length parameter L from a fit for "confined" trajectory ($\mu_2(t) = 4\sigma^2 + \frac{L^2}{3}\left[1 - e^{-12Dt/L^2}\right]$). Transient arrest of diffusion (TAD) analysis consists in evaluating the probability for a certain point in a trajectory to be in a transient confinement zone (TCZ), i.e. if the particle (within a time-window up to a maximum of S_m steps around the considered frame) is confined in a zone that is smaller than expected given the average D of the whole trajectory; the trajectory is then divided in "diffusive" and "confined" subtrajectories. This analysis was considered for non-self-similar trajectories, and was carried out as in (Simson et al., 1995), considering S_m of 18 steps, a critical minimum threshold value of the probability level L_{TCZ} of being within a TCZ (Simson et al., 1995) L_c=2.5, and a minimal duration t_c of 8 steps for the TCZ candidates to be considered real TCZs. Obtained (sub)trajectories were classified as shown in the diagram according to the values of the previously cited parameters and considering that immobile ones can produce fit parameters and uncertainties outside reasonable limits, being the localization uncertainty much

higher than the real movement of the particle, checking therefore also the results of TAD analysis. The parameters for the classification were optimized on the basis of careful inspection of the results on Qdots-labelled TrkA receptors within cells untreated or treated with NGF. Consecutive subtrajectories classified as fast, or non-fast-diffusing, were considered as a single one; TAD events are slow and/or immobile trajectory parts between fast ones. All the distributions and data reported throughout this work were then calculated automatically from the final (sub)trajectories. The Refs. cited here appear also in the main text.

Supplementary Tables

	Multimodal trajectories					Diffusive parts				TAD events				
Treatment	**#multi**	**subtraj /multi**	**multi %**	**D ($\mu m^2/s$)**	**ΔD ($\mu m^2/s$)**	**Time%**	**‹t› (s)**	**D ($\mu m^2/s$)**	**ΔD ($\mu m^2/s$)**	**Time%**	**‹t› (s)**	**τ (s)**	**D ($\mu m^2/s$)**	**ΔD ($\mu m^2/s$)**
TrkA untreated	112	3.9	34	0.41	0.23	79	6.8	0.48	0.24	21	2.4	0.4	0.04	0.07
TrkA +NGF	123	4.1	28	0.25	0.22	47	6.5	0.38	0.23	53	7.9	0.4	0.03	0.05
TrkA +NGF R100E	159	4.9	32	0.23	0.18	48	6.0	0.33	0.20	52	6.6	0.4	0.03	0.08
TrkA +proNGF	173	4.5	34	0.32	0.21	56	5.7	0.42	0.22	44	5.0	0.4	0.03	0.04
TrkA +NT-3	221	5.5	46	0.26	0.16	70	4.8	0.34	0.17	30	2.3	0.6	0.04	0.08
TrkA+K252a	121	4.4	34	0.23	0.19	55	5.8	0.35	0.19	45	5.0	0.5	0.03	0.05
TrkA+K252a +NGF	306	4.5	34	0.28	0.17	68	6.7	0.35	0.18	32	3.8	0.5	0.03	0.07
TrkA+Chlprz	202	4.3	43	0.27	0.17	75	5.1	0.34	0.19	25	2.2	0.5	0.03	0.10
TrkA+Chlprz +NGF	269	4.0	39	0.23	0.13	67	4.9	0.30	0.15	33	2.9	0.6	0.04	0.12
TrkA+CytD	223	4.0	41	0.21	0.15	55	5.1	0.31	0.19	45	4.5	0.9	0.03	0.08
TrkA+CytD +NGF	87	5.1	31	0.19	0.15	50	5.1	0.31	0.18	50	5.3	0.6	0.03	0.06

Table S1. Quantitative parameters describing ACP-TrkA multimodal trajectories in response to different stimuli. #multi: number of multimodal trajectories detected; subtrajs/multi: average number of subtrajectories coming from a single multimodal trajectory; multi%: ratio % of the number of multimodal trajectories over the total number of analyzed trajectories; D and ΔD: mean and population standard deviation for the distribution of the short-lag-time diffusion coefficient D calculated for multimodal trajectories and for their diffusive or confined subtrajectories: Time%: total time fraction for the subtrajectory type on the total time of multimodal trajectories; ‹*t*› average trajectory time length; τ: parameter of exponential fit of the distribution of the time lengths of the trajectories (calculated for TAD events in order to reduce the impact of long slow or immobile subtrajectories that were actually the most part of a trajectory; in the other case it is not significantly different from ‹*t*›). We did not observe a clear trend in the parameters characterizing the multimodal trajectories with the treatment, except the (long) average time ‹*t*› of TAD events; this is however impacted mainly by multimodal trajectories that are mostly confined or slow, with some escaping events; these are not the type of subtrajectories previously typically studied with similar analysis (Simson et al., 1995, Suzuki et al., 2007), and can be linked to the formation of endosome precursors on the basal membrane. Indeed, ‹*t*› for TAD events is smaller in the cases where the impact of endosome precursors is minimized, *i.e.* in the untreated samples, the ones treated with NT3 and the one treated with Chlorpromazine, which inhibits their formation.

	region 1 %	region 2 %	region 3 %	region 4 %	region 5 %	region 6 %	region 7 %	region 8 %
TrkA	65.6	6.6	6.2	1.5	0.3	0.2	4.3	2.7
TrkA+NGF	27.8	13.2	11.6	6.3	7.5	12.5	1.2	3.0
TrkA+NGF R100E	30.5	12.2	18.1	5.9	5.1	6.9	1.6	2.8
TrkA +proNGF	50.0	7.2	15.6	2.3	1.4	6.4	1.7	1.9
TrkA +NT-3	58.9	4.0	7.9	3.7	3.5	2.8	2.0	2.2
TrkA +K252a	43.5	7.7	15.0	4.3	1.8	5.9	1.8	4.9
TrkA +K252a+NGF	56.0	3.5	9.5	4.6	1.1	6.8	2.8	2.2
TrkA +Chlprz	69.3	2.0	3.6	2.5	1.1	4.0	3.8	1.7
TrkA +Chlprz+NGF	51.4	2.7	7.2	6.5	4.1	4.6	3.7	2.7
TrkA +CytD	35.2	5.4	15.9	6.7	2.1	9.0	2.4	3.1
TrkA +CytD+NGF	21.4	7.3	19.2	13.9	2.7	12.9	1.4	3.7

Table S2

Frequency % of different dynamics modes for ACP-TrkA receptors, as calculated from the integral of the experimental *D*-γ distribution in the eight numbered regions shown in Figures 4 and 5 (and reported also in Fig. S6), describing ACP-TrkA single molecule dynamics in response to different stimuli; the values in each row do not sum up to 100% since the 8 regions do not cover the whole domain considered for the *D*-γ distributions.